Chapter 2
Downlink Synchronization

Qi Wang

In this chapter, we present a framework for link performance evaluation of a Long Term Evolution (LTE) downlink with imperfect carrier frequency synchronization. This framework interconnects three performance metrics, namely mean squared error of the carrier frequency offset estimation, post-equalization signal-to-interference-plus-noise ratio, and eventually bit-interleaved coded modulation capacity. With the presented framework, the throughput loss from a residual Carrier Frequency Offset (CFO) estimation error can be analytically determined, given standardized OFDM transmission parameters. In order to validate this mathematical model, extensive link level simulations were carried out using a standard compliant LTE link level simulator. The comparison between the calculated and the simulated results exhibits a fair agreement. This model on the one hand exposes the CFO-tolerance of a standardized OFDM transmission system; on the other hand, it may serve as a means for evaluating CFO estimation algorithms designed for the LTE downlink.[1]

2.1 Introduction

As a dominant physical layer technique in the next generation wireless communication standard, 3GPP LTE, Orthogonal Frequency Division Multiplexing (OFDM) promises significant performance gain in frequency selective channels. Nevertheless, it poses a drawback, namely, sensitive to synchronization errors, such as CFO,

[1]More details on synchronization issues can be found in the Ph.D. thesis of Qi Wang, available at http://theses.eurasip.org/theses/470/performance-evaluation-of-practical-ofdm-systems/download/.

This work has been carried out while she was at the Institute of Telecommunications, TU Wien.

Q. Wang (✉)
Huawei Technologies Düsseldorf GmbH, Düsseldorf, Germany
e-mail: wangqiasia@gmail.com

M. Rupp et al., *The Vienna LTE-Advanced Simulators*,
Signals and Communication Technology, DOI 10.1007/978-981-10-0617-3_2

sampling frequency offset and symbol timing offset. Tremendous efforts were devoted to estimating synchronization errors in the digital signal processing domain. Taking the CFO for example, the performance is evaluated in terms of the Mean Square Error (MSE). Such a metric indicates the estimation performance itself, yet fails to reflect the influence of a residual estimation error on the overall system performance. In a real world communication system, the physical layer performance is eventually expressed in terms of coded throughput. Therefore, not only the performance of an individual processing block but also their overall impact on the throughput needs to be investigated.

For an OFDM system in general, the performance degradation caused by a CFO has been investigated in [1–8]. The authors of [1, 2] evaluated the degradation in terms of the Signal to Interference and Noise Ratio (SINR) in the demodulated OFDM signal. In [3–8], Bit Error Ratio (BER) of OFDM systems with CFO was analytically derived for Additive White Gaussian Noise (AWGN) [3–5] and frequency selective fading channel [6]. In [8], a capacity analysis of impaired OFDM links is presented, taking into account a variety of receiver imperfections, e.g., channel estimation errors, CFO and I/Q imbalance. The authors calculated the average mutual information of the impaired OFDM link using the probability density function derived in [7]. From a methodology point of view, these approaches evaluate the degradation induced by the Inter-Carrier Interference (ICI) exclusively and are applicable to an arbitrary OFDM system; whereas in order to evaluate a standardized system like LTE, many practical aspects need to be taken into account, such as the specified frame structure and the overall receiver design.

Performance modeling has become of interest as nowadays communication systems grow dramatically in complexity. Since simulating a perfect replica of the real system turns to be costly in terms of run time efficiency, it is necessary to combine mathematical and empirical models in the simulation-based performance evaluation. In order to reduce the simulation complexity without losing insight into the real behavior, modeling with an acceptable degree of approximations is desired. For the LTE downlink, a link quality modeling approach has been presented in [9, 10]. The authors derived bounds on achievable throughput of LTE where the post-equalization SINR was employed as the intermediate performance metric. This approach can be utilized to abstract the major physical layer behavior, whereas synchronization errors were ignored.

We apply the methodology elaborated in [9] and develop a throughput loss prediction model for the CFO impaired LTE downlink. This model takes into account the estimation performance of a CFO estimator, a linear receiver structure as well as the Bit Interleaved Coded Modulation (BICM) architecture and analytically determines the performance loss in terms of coded throughput. Validated by extensive standard compliant simulations, this evaluation model on the one hand exposes the CFO-tolerance of such a system; on the other hand, implies how accurate the carrier frequency offset estimation is required to be.

The chapter is organized as follows. A description of the evaluation model is presented in Sect. 2.2. The MSE performance of an exemplified CFO estimator is described in Sect. 2.3. The post-equalization SINR model for a CFO-impaired OFDM transmission is derived in Sect. 2.4. The BICM capacity model is briefly introduced in Sect. 2.5. Numerical validations using the standard compliant Vienna LTE Link-Level DL simulator are provided in Sect. 2.6. Conclusion can be found in Sect. 2.7.

2.2 Evaluation Model

Consider a signal processing chain on the receiver side of the LTE downlink in Fig. 2.1, the frequency synchronization block is located at the beginning of the processing chain, compensating the CFO in the time domain. In order to model the impact of a residual CFO on the resulting coded throughput at the end of the chain, analytical representations need to be found for the function blocks in between.

The signal transmission in LTE is based on a frame structure, illustrated in Fig. 2.2. The transmission resources are segmented into 10 ms frames. Each frame is divided into ten subframes. When a Cyclic Prefix (CP) of normal length is employed, a subframe consists of 14 OFDM symbols [11]. The frame structure is designed so that the signaling information can be embedded on a certain basis with a reasonable overhead. After the Fast Fourier Transform (FFT) transform, the transmission resource can be interpreted as a time-frequency grid, where Reference Signals (RSs) are embedded among data symbols.

Since the post-equalization SINR has been widely utilized for evaluating the performance of a radio link, we choose it as an intermediate step to evaluate the entire receiver chain, i.e.,

$$\text{MSE} \rightarrow \text{post-equalization SINR} \rightarrow \text{coded throughput.}$$

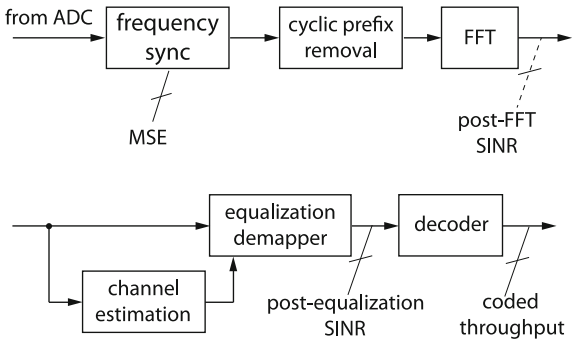

Fig. 2.1 Signal processing chain in an OFDM receiver

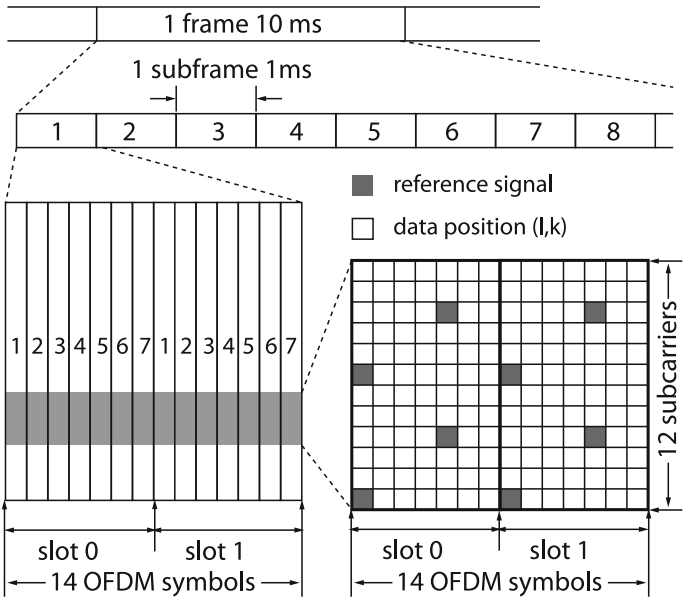

Fig. 2.2 LTE frame structure with normal length CPs, displaying a time-frequency grid in the frequency domain with RS positions

Typically, optimizations are applied based on MSE, assuming an overall optimal can be correspondingly achieved. Our analysis however, will provide an insight by modeling the joint effect of the three.

2.3 Mean Square Error of Carrier Frequency Offset Estimation

In order to compensate the CFO in a real-world OFDM transmission system, various CFO estimation schemes can be applied. Their estimation performances in terms of MSE can be mathematically determined. In [12], a generic CFO estimation scheme was investigated based on the RSs of LTE, where the normalized CFO $\varepsilon \in (-0.5, 0.5)$ is estimated firstly in the time domain then refined in the frequency domain. We focus on the frequency domain estimation in the following because it determines the overall estimation performance. Define vectors $\mathbf{r}_{\mathscr{P},0}, \mathbf{r}_{\mathscr{P},1} \in \mathbb{C}^{N_{\mathrm{P}}N_{\mathrm{R}}\times 1}$ for the received RS in slot 0 and 1, diagonal matrices $\mathbf{X}_0 = \mathrm{diag}\left(\mathbf{x}_{\mathscr{P},0}\right), \mathbf{X}_1 = \mathrm{diag}\left(\mathbf{x}_{\mathscr{P},1}\right) \in \mathbb{C}^{N_{\mathrm{P}}N_{\mathrm{R}}\times N_{\mathrm{P}}N_{\mathrm{R}}}$ containing the corresponding RSs along their diagonals. The CFO is estimated in the frequency domain by

$$\hat{\varepsilon} = -\frac{N_{\mathrm{c}}}{2\pi(N_{\mathrm{c}}+N_{\mathrm{cp}})N_{\mathrm{sl}}} \arg\left\{\mathbf{r}_{\mathscr{P},1}^{\mathrm{H}}\mathbf{X}_1\mathbf{X}_0^{\mathrm{H}}\mathbf{r}_{\mathscr{P},0}\right\}, \tag{2.1}$$

where $N_{\mathrm{sl}} \in \{6, 7\}$ is the number of OFDM symbols per slot and N_{P} is the number of RSs per slot. We consider this estimation scheme as an example and evaluate the throughput loss of a CFO-impaired LTE downlink with this estimation scheme employed.

The MSE of the overall CFO estimation scheme is given as

$$\mathrm{MSE}(\gamma) = \mathbb{E}\left\{|\varepsilon - \hat{\varepsilon}|^2\right\} = \frac{N_{\mathrm{c}}^2}{4\pi^2(N_{\mathrm{c}}+N_{\mathrm{cp}})^2 N_{\mathrm{sl}}^2 N_{\mathrm{R}} N_{\mathrm{P}}\gamma}, \tag{2.2}$$

The variable γ denotes the average Signal to Noise Ratio (SNR) at the receiver side in the frequency domain.

The estimation performance of the generic difference phase estimator has been thoroughly analyzed in [13]. A derivation of Eq. (2.2) following the work in [12] is provided. Define the channel frequency response on the RS subcarriers as $\mathbf{h} \in \mathbb{C}^{N_{\mathrm{P}}N_{\mathrm{R}}\times 1}$; the received RS symbols in slot 0 and 1 can be expressed as

$$\mathbf{r}_{\mathscr{P},0} = \mathbf{X}_0\mathbf{h} + \mathbf{v}_0, \tag{2.3}$$

$$\mathbf{r}_{\mathscr{P},1} = \mathrm{e}^{\mathrm{i}\cdot\phi N_{\mathrm{sl}}}\mathbf{X}_1\mathbf{h} + \mathbf{v}_1, \tag{2.4}$$

where $\mathbf{v}_0, \mathbf{v}_1$ denote the corresponding noise vectors and $\phi = \frac{2\pi\varepsilon(N_{\mathrm{c}}+N_{\mathrm{cp}})}{N_{\mathrm{c}}}$. From Eq. (2.1), there is

$$\begin{aligned}\mathbf{r}_{\mathscr{P},1}^{\mathrm{H}}\mathbf{X}_1\mathbf{X}_0^{\mathrm{H}}\mathbf{r}_{\mathscr{P},0} = {} & \mathrm{e}^{-\mathrm{i}\cdot\phi N_{\mathrm{sl}}}\mathbf{h}^{\mathrm{H}}\mathbf{X}_1^{\mathrm{H}}\mathbf{X}_1\mathbf{X}_0^{\mathrm{H}}\mathbf{X}_0\mathbf{h} \\ & + \mathrm{e}^{-\mathrm{i}\cdot\phi N_{\mathrm{sl}}}\mathbf{h}^{\mathrm{H}}\mathbf{X}_1^{\mathrm{H}}\mathbf{X}_1\mathbf{X}_0^{\mathrm{H}}\mathbf{v}_0 + \mathbf{v}_1^{\mathrm{H}}\mathbf{X}_1\mathbf{X}_0^{\mathrm{H}}\mathbf{X}_0\mathbf{h} \\ & + \mathbf{v}_1^{\mathrm{H}}\mathbf{X}_1\mathbf{X}_0^{\mathrm{H}}\mathbf{v}_0.\end{aligned} \tag{2.5}$$

Omitting the second-order noise term $\mathbf{v}_1^{\mathrm{H}}\mathbf{X}_1\mathbf{X}_0^{\mathrm{H}}\mathbf{v}_0$, $\mathbf{r}_{\mathscr{P},1}^{\mathrm{H}}\mathbf{X}_1\mathbf{X}_0^{\mathrm{H}}\mathbf{r}_{\mathscr{P},0}$ can be approximated as a complex Gaussian random variable, expressed as

$$\mathbf{r}_{\mathscr{P},1}^{\mathrm{H}}\mathbf{X}_1\mathbf{X}_0^{\mathrm{H}}\mathbf{r}_{\mathscr{P},0} \sim \mathscr{N}_{\mathbb{C}}\left(\mathrm{e}^{-\mathrm{i}\phi N_{\mathrm{sl}}}P_{\mathrm{S}}^2\mathbf{h}^{\mathrm{H}}\mathbf{h}, 2P_{\mathrm{V}}P_{\mathrm{S}}^3\mathbf{h}^{\mathrm{H}}\mathbf{h}\right), \tag{2.6}$$

where P_{S} and P_{V} denote the signal and noise power, respectively. Define

$$Y, X \sim \mathscr{N}_{\mathbb{C}}\left(0, P_{\mathrm{V}}P_{\mathrm{S}}^3\mathbf{h}^{\mathrm{H}}\mathbf{h}\right), \tag{2.7}$$

and assume $-\frac{\pi}{2} < \phi N_{\mathrm{sl}} < \frac{\pi}{2}$, Eq. (2.1) becomes

$$\begin{aligned}\hat{\phi} &= -\frac{1}{N_{\mathrm{sl}}} \arctan\left\{\frac{\Im\left\{\mathbf{r}_{\mathscr{P},1}^{\mathrm{H}}\mathbf{X}_1\mathbf{X}_0^{\mathrm{H}}\mathbf{r}_{\mathscr{P},0}\right\}}{\Re\left\{\mathbf{r}_{\mathscr{P},1}^{\mathrm{H}}\mathbf{X}_1\mathbf{X}_0^{\mathrm{H}}\mathbf{r}_{\mathscr{P},0}\right\}}\right\} \\ &= -\frac{1}{N_{\mathrm{sl}}} \arctan\left\{\frac{P_{\mathrm{S}}^2\mathbf{h}^{\mathrm{H}}\mathbf{h}\cdot\sin(-\phi N_{\mathrm{sl}}) + Y}{P_{\mathrm{S}}^2\mathbf{h}^{\mathrm{H}}\mathbf{h}\cdot\cos(-\phi N_{\mathrm{sl}}) + X}\right\} \\ &\approx -\frac{1}{N_{\mathrm{sl}}} \arctan\left\{\frac{P_{\mathrm{S}}^2\mathbf{h}^{\mathrm{H}}\mathbf{h}\cdot\sin(-\phi N_{\mathrm{sl}})}{P_{\mathrm{S}}^2\mathbf{h}^{\mathrm{H}}\mathbf{h}\cdot\cos(-\phi N_{\mathrm{sl}})}\right\} \\ &\quad - \frac{1}{N_{\mathrm{sl}}}\cdot\frac{Y\cos(-\phi N_{\mathrm{sl}}) - X\sin(-\phi N_{\mathrm{sl}})}{P_{\mathrm{S}}^2\mathbf{h}^{\mathrm{H}}\mathbf{h}} \\ &= \phi - \frac{1}{N_{\mathrm{sl}}}\cdot\frac{Y\cos(-\phi N_{\mathrm{sl}}) - X\sin(-\phi N_{\mathrm{sl}})}{P_{\mathrm{S}}^2\mathbf{h}^{\mathrm{H}}\mathbf{h}}\end{aligned} \tag{2.8}$$

by applying a first-order Taylor expansion. Plugging in Eq. (2.7), we obtain

$$\begin{aligned}\hat{\phi} &\sim \mathscr{N}_{\mathbb{C}}\left(\phi, \frac{P_{\mathrm{V}}P_{\mathrm{S}}^3\mathbf{h}^{\mathrm{H}}\mathbf{h}\cos^2(-\phi N_{\mathrm{sl}}) + P_{\mathrm{V}}P_{\mathrm{S}}^3\mathbf{h}^{\mathrm{H}}\mathbf{h}\sin^2(-\phi N_{\mathrm{sl}})}{N_{\mathrm{sl}}^2P_{\mathrm{S}}^4\mathbf{h}^{\mathrm{H}}\mathbf{h}\mathbf{h}^{\mathrm{H}}\mathbf{h}}\right) \\ &\sim \mathscr{N}_{\mathbb{C}}\left(\phi, \frac{P_{\mathrm{V}}}{N_{\mathrm{sl}}^2P_{\mathrm{S}}\mathbf{h}^{\mathrm{H}}\mathbf{h}}\right).\end{aligned} \tag{2.9}$$

Therefore, the estimator is unbiased and

$$\begin{aligned}\mathrm{MSE}(\gamma) &= \mathbb{E}\left\{|\varepsilon - \hat{\varepsilon}|^2\right\} = \frac{N_{\mathrm{c}}^2}{4\pi^2(N_{\mathrm{c}}+N_{\mathrm{cp}})^2}\mathbb{E}\left\{|\phi - \hat{\phi}|^2\right\} \\ &= \frac{N_{\mathrm{c}}^2P_{\mathrm{V}}}{4\pi^2(N_{\mathrm{c}}+N_{\mathrm{cp}})^2N_{\mathrm{sl}}^2P_{\mathrm{S}}\mathbf{h}^{\mathrm{H}}\mathbf{h}} = \frac{N_{\mathrm{c}}^2}{4\pi^2(N_{\mathrm{c}}+N_{\mathrm{cp}})^2N_{\mathrm{sl}}^2N_{\mathrm{P}}N_{\mathrm{R}}\gamma},\end{aligned} \tag{2.10}$$

where the average SNR

$$\gamma = \frac{P_{\mathrm{S}}\mathbf{h}^{\mathrm{H}}\mathbf{h}}{N_{\mathrm{P}}N_{\mathrm{R}}P_{\mathrm{V}}}. \tag{2.11}$$

In classical estimation theory, the MSE of an unbiased estimator for ε is lower bounded as

$$\mathrm{MSE}_{\varepsilon} = \frac{N_{\mathrm{c}}^2}{4\pi^2(N_{\mathrm{c}}+N_{\mathrm{cp}})^2}\mathrm{MSE}_{\phi} \geq \frac{N_{\mathrm{c}}^2}{4\pi^2(N_{\mathrm{c}}+N_{\mathrm{cp}})^2}\cdot\frac{1}{J(\phi)}, \tag{2.12}$$

where the Fisher information

$$J(\phi) = -\mathbb{E}\left\{\frac{\partial^2}{\partial\phi^2}\Lambda(\phi)\right\}. \tag{2.13}$$

Given the notation in Eqs. (2.3) and (2.4), we characterize the RS-based CFO estimation problem by the log-likelihood function

$$\begin{aligned}\Lambda(\phi) &= \ln f(\mathbf{r}_{\mathscr{P},0}, \mathbf{r}_{\mathscr{P},1}; \phi) \\ &= \ln \frac{1}{\pi^{2N_\mathrm{P}N_\mathrm{R}} \det(\mathbf{R})} \exp\left\{ - \begin{bmatrix} \mathbf{r}_{\mathscr{P},0}^\mathrm{H} & \mathbf{r}_{\mathscr{P},1}^\mathrm{H} \end{bmatrix} \mathbf{R}^{-1} \begin{bmatrix} \mathbf{r}_{\mathscr{P},0} \\ \mathbf{r}_{\mathscr{P},1} \end{bmatrix} \right\},\end{aligned} \tag{2.14}$$

with

$$\mathbf{R} = \mathbb{E}\left\{ \begin{bmatrix} \mathbf{r}_{\mathscr{P},0} \\ \mathbf{r}_{\mathscr{P},1} \end{bmatrix} \begin{bmatrix} \mathbf{r}_{\mathscr{P},0}^\mathrm{H} & \mathbf{r}_{\mathscr{P},1}^\mathrm{H} \end{bmatrix} \right\}. \tag{2.15}$$

Plugging Eqs. (2.3) and (2.4) into (2.14), after arithmetic manipulations, Eq. (2.13) becomes

$$J(\phi) = \frac{N_\mathrm{sl}^2 P_\mathrm{S} \mathbf{h}^\mathrm{H}\mathbf{h}}{P_\mathrm{V}}. \tag{2.16}$$

This leads to the Cramér-Rao Lower Bound (CRLB)

$$\begin{aligned}\mathrm{MSE}_\varepsilon &\geq \frac{N_\mathrm{c}^2 P_\mathrm{V}}{4\pi^2 (N_\mathrm{c} + N_\mathrm{cp})^2 N_\mathrm{sl}^2 P_\mathrm{S} \mathbf{h}^\mathrm{H}\mathbf{h}} \\ &= \frac{N_\mathrm{c}^2}{4\pi^2 (N_\mathrm{c} + N_\mathrm{cp})^2 N_\mathrm{sl}^2 N_\mathrm{P} N_\mathrm{R} \gamma}.\end{aligned} \tag{2.17}$$

Compared to Eq. (2.10), the lower bound of the estimation variance is attained.

2.4 Signal to Interference and Noise Ratio Modeling

The authors of [1, 2] investigated the impact of a CFO on OFDM systems where such impact means exclusively the degradation in terms of the post-FFT SINR, shown in Fig. 2.1. In [14], a post-equalization SINR model was presented. This measure is of importance, because it directly determines the theoretically possible throughput I via Shannon's formula:

$$I \approx \log_2(1 + \mathrm{SINR}). \tag{2.18}$$

In an urban scenario with low to medium mobility, it can be shown that the channel is quasi-static within the duration of one subframe (1 ms). Therefore, time-invariant channel estimation and equalization can be applied on a subframe basis. Following the analysis in [14], we constrain the evaluation within one subframe and consider a residual CFO which is normalized to the standardized subcarrier spacing, denoted

by $\varepsilon \in (-0.5, 0.5)$. Let n be the OFDM symbol index within a subframe, k the subcarrier index, N_T the number of transmit antennas and N_R the number of receive antennas. We denote the transmitted signal vector by $\mathbf{x}_{n,k} \in \mathbb{C}^{N_\mathrm{L}\times 1}$, the precoded channel matrix in the frequency domain by $\mathbf{H}_k^{(\mathrm{eff})} \in \mathbb{C}^{N_\mathrm{R}\times N_\mathrm{L}}$, the received signal by $\mathbf{r}_{n,k} \in \mathbb{C}^{N_\mathrm{R}\times 1}$ and the AWGN by $\mathbf{v}_{n,k} \in \mathbb{C}^{N_\mathrm{R}\times 1}$. We use here the abbreviation $\mathbf{H}_k^{(\mathrm{eff})} = \mathbf{H}_k\mathbf{F}_k$, where the channel matrix $\mathbf{H}_k \in \mathbb{C}^{N_\mathrm{R}\times N_\mathrm{T}}$ and the precoding matrix $\mathbf{F}_k \in \mathbb{C}^{N_\mathrm{T}\times N_\mathrm{L}}$. Given the block fading assumption, the channel matrix within one subframe stays constant, independent from the OFDM symbol index n. When the system is impaired by a CFO, the signal transmission can be described as

$$\begin{aligned}\mathbf{r}_{n,k} &= I(0,\varepsilon)\cdot \mathrm{e}^{\mathrm{i}\Phi(\varepsilon,n)}\cdot \mathbf{H}_k^{(\mathrm{eff})}\mathbf{x}_{n,k} \\ &\quad + \sum_{p\neq k} I(p-k,\varepsilon)\cdot \mathrm{e}^{\mathrm{i}\Phi(\varepsilon,n)}\cdot \mathbf{H}_p^{(\mathrm{eff})}\mathbf{x}_{n,p} + \mathbf{v}_{n,k},\end{aligned} \tag{2.19}$$

where

$$I(0,\varepsilon) = \frac{\sin(\pi\varepsilon)}{N_\mathrm{c}\sin(\pi\varepsilon/N_\mathrm{c})}\cdot \mathrm{e}^{\mathrm{i}\frac{\pi\varepsilon(N_\mathrm{c}-1)}{N_\mathrm{c}}}, \tag{2.20}$$

$$I(p-k,\varepsilon) = \frac{\sin[\pi(p-k+\varepsilon)]}{N_\mathrm{c}\sin[\pi(p-k+\varepsilon)/N_\mathrm{c}]}\cdot \mathrm{e}^{\mathrm{i}\frac{\pi(p-k+\varepsilon)(N_\mathrm{c}-1)}{N_\mathrm{c}}}, \tag{2.21}$$

$$\mathrm{e}^{\mathrm{i}\Phi(\varepsilon,n)} = \mathrm{e}^{\mathrm{i}\frac{2\pi\varepsilon n(N_\mathrm{c}+N_\mathrm{cp})}{N_\mathrm{c}}}. \tag{2.22}$$

Here, the factor $I(0,\varepsilon)\cdot \mathrm{e}^{\mathrm{i}\Phi(\varepsilon,n)}$ introduces time-variant distortion to the desired signal term besides the channel response. However, since the system is assumed on a subframe basis to be static, the receiver is designed to be time invariant on a subframe basis; in other words, a universal channel estimate which is independent of the time index n is to be obtained using all RSs shown in Fig. 2.2.

For simplicity, we assume that the perfect and static channel knowledge is available at each subframe. A Zero Forcing (ZF) equalizer at subcarrier k is then given as

$$\mathbf{G}_k = \left(\mathbf{H}_k^{(\mathrm{eff})\mathrm{H}}\mathbf{H}_k^{(\mathrm{eff})}\right)^{-1}\mathbf{H}_k^{(\mathrm{eff})\mathrm{H}}. \tag{2.23}$$

Thus, the estimated data symbol after equalization can be expressed as

$$\begin{aligned}\hat{\mathbf{x}}_{n,k} &= \mathbf{G}_k\cdot\mathbf{r}_{n,k} = I(0,\varepsilon)\cdot \mathrm{e}^{\mathrm{i}\Phi(\varepsilon,n)}\cdot\mathbf{x}_{n,k} \\ &\quad + \underbrace{\mathbf{G}_k\sum_{p\neq k} I(p-k,\varepsilon)\cdot \mathrm{e}^{\mathrm{i}\Phi(\varepsilon,n)}\cdot \mathbf{H}_p^{(\mathrm{eff})}\mathbf{x}_{l,p}}_{\mathbf{y}_{n,k}^{\mathrm{ICI}}} + \underbrace{\mathbf{G}_k\mathbf{v}_{n,k}}_{\tilde{\mathbf{v}}_{n,k}} \\ &= I(0,\varepsilon)\cdot \mathrm{e}^{\mathrm{i}\Phi(\varepsilon,n)}\cdot\mathbf{x}_{n,k} + \mathbf{y}_{n,k}^{\mathrm{ICI}} + \tilde{\mathbf{v}}_{n,k},\end{aligned} \tag{2.24}$$

where $\mathbf{y}_{n,k}^{\mathrm{ICI}}$ denotes the ICI and $\tilde{\mathbf{v}}_{n,k}$ is the equalized noise vector. Let N_{L} denote the number of transmission layers which is indexed by $l = 0, 1, \ldots, N_{\mathrm{L}} - 1$, the $\mathrm{SINR}_{n,k}^{(l)}$ on the lth layer can be found by

$$\mathrm{SINR}_{n,k}^{(l)}(\varepsilon, \mathbf{H}_k^{(\mathrm{eff})}) = \frac{\left[\mathbf{x}_{n,k}\mathbf{x}_{n,k}^{\mathrm{H}}\right]_{(l,l)}}{\left[(\hat{\mathbf{x}}_{n,k} - \mathbf{x}_{n,k})(\hat{\mathbf{x}}_{n,k} - \mathbf{x}_{n,k})^{\mathrm{H}}\right]_{(l,l)}}, \tag{2.25}$$

where $[\,\cdot\,]_{(i,j)}$ denotes the entry on the ith row and jth column of the given matrix. We denote the average signal power on each subcarrier and each layer by P_{S} and the corresponding noise power by P_{V}. Plugging Eq. (2.24) into (2.25), we obtain a closed form expression of the post-equalization SINR on the lth layer at Resource Element (RE) (n, k), shown in Eq. (2.27). Since the system assumes block fading on a subframe bases, the so-called Common Phase Error (CPE) in Eq. (2.22) which increases linearly with the time index n causes a signal distortion term. As suggested in [14], this is the dominant term compared to the ICI.

$$\begin{aligned}
&\mathrm{SINR}_{n,k}^{(l)}(\varepsilon, \mathbf{H}_k^{(\mathrm{eff})}) \qquad (2.26)\\
&= \frac{P_{\mathrm{S}}}{\left[\mathbf{y}_{n,k}^{\mathrm{ICI}}\mathbf{y}_{n,k}^{\mathrm{ICI}\,\mathrm{H}}\right]_{(l,l)} + \left[\tilde{\mathbf{v}}_{n,k}\tilde{\mathbf{v}}_{n,k}^{\mathrm{H}}\right]_{(l,l)} + |I(0,\varepsilon)\cdot \mathrm{e}^{\mathrm{i}\Phi(\varepsilon,n)} - 1|^2 \cdot \left[\mathbf{x}_{n,k}\mathbf{x}_{n,k}^{\mathrm{H}}\right]_{(l,l)}}\\
&= \frac{P_{\mathrm{S}}}{\mathrm{ICI} + \underbrace{P_{\mathrm{V}}\left[\mathbf{G}_k^{\mathrm{H}}\mathbf{G}_k\right]_{(l,l)}}_{\text{noise}} + \underbrace{P_{\mathrm{S}}|I(0,\varepsilon)\cdot \mathrm{e}^{\mathrm{i}\Phi(\varepsilon,n)} - 1|^2}_{\text{signal distortion}}}, \qquad (2.27)
\end{aligned}$$

$$\mathrm{ICI} = P_{\mathrm{S}} \sum_{p \neq k} |I(p-k,\varepsilon)|^2 \left[\mathbf{G}_k^{\mathrm{H}}\mathbf{G}_k\mathbf{H}_p^{(\mathrm{eff})}\mathbf{H}_p^{(\mathrm{eff})\,\mathrm{H}}\right]_{(l,l)}. \tag{2.28}$$

2.5 Bit Interleaved Coded Modulation Capacity

In general, a BICM architecture is obtained by concatenating channel coding with modulation mapping through a bit interleaver. Such a scheme allows combinations of any channel code with any arbitrary modulation alphabet [15]. Based on this architecture, LTE employs 4, 16 or 64-Quadrature Amplitude Modulation (QAM) and a rate 1/3 turbo code that is appropriately rate matched to achieve the desired code rates as defined in [16]. The capacity of BICM systems is well known, though not in closed-form [17]. In Fig. 2.3, BICM capacity of the three LTE-defined modulation alphabets (4-QAM, 16-QAM, 64-QAM) are plotted. Analogous to [10], a function $f(\mathrm{SINR})$ is introduced to describe the maximum efficiency over all available modulation alphabets.

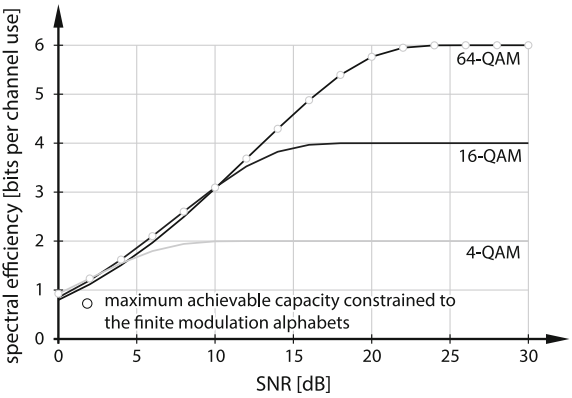

Fig. 2.3 BICM capacity of 4, 16 and 64-QAM modulation

Given the SINR model in Sect. 2.2, the spectral efficiency of an LTE downlink transmission suffering from a CFO ε can be expressed as $f(\mathrm{SINR}_{n,k}^{(l)}(\varepsilon, \mathbf{H}_k^{(\mathrm{eff})}))$, where $\mathrm{SINR}_{n,k}^{(l)}(\varepsilon, \mathbf{H}_k^{(\mathrm{eff})})$ is plugged in from Eq. (2.27). The index (n, k) denotes an RE which is devoted to data transmission; in other words, overhead such as RSs, Primary Synchronization Signal (PSS), Secondary Synchronization Signal (SSS) and guard bands are excluded. Therefore, the average spectral efficiency that can be achieved at each transmission layer is written as

$$\bar{B}(\varepsilon) = \frac{1}{N_{\mathrm{D}} N_{\mathrm{L}}} \sum_{(n,k)} \sum_{l} f(\mathrm{SINR}_{n,k}^{(l)}(\varepsilon, \mathbf{H}_k^{(\mathrm{eff})})), \tag{2.29}$$

where N_{D} is the number of available data REs.

Given the MSE analysis in Sect. 2.3, a theoretical residual estimation error can be assumed, labeled as $\bar{\varepsilon} = \sqrt{\mathrm{MSE}(\gamma)}$. Thus, a theoretically achievable BICM capacity can be expressed as

$$\begin{aligned} B(\gamma) &= \sum_{(n,k)} \sum_{l} f(\mathrm{SINR}_{n,k}^{(l)}(\bar{\varepsilon}, \mathbf{H}_k^{(\mathrm{eff})})) \\ &= \sum_{(n,k)} \sum_{l} f(\mathrm{SINR}_{n,k}^{(l)}(\sqrt{\mathrm{MSE}(\gamma)}, \mathbf{H}_k^{(\mathrm{eff})})). \end{aligned} \tag{2.30}$$

This capacity bound takes into account the finite set of Modulation and Coding Schemes (MCSs) suggested in [16], a linear receiver structure and the limitation of the CFO estimation performance, while it ignores other aspects such as a suboptimal channel coding, selection of suitable precoding matrix and number of transmit streams. Since we are only interested in the throughput difference between the

zero-CFO case and the CFO-compensated case, these imperfect modeling aspects cause the same effect in both cases. The throughput loss, being the difference of them two, can be calculated as

$$\Delta B(\gamma) = \sum_{(n,k)} \sum_{l} f(\mathrm{SINR}_{n,k}^{(l)}(0, \mathbf{H}_k^{(\mathrm{eff})})) - B(\gamma). \tag{2.31}$$

2.6 Numerical Results

In this section, we validate the analytical models presented in Sects. 2.3, 2.4 and 2.5 by standard compliant simulations of LTE downlink using the *Vienna LTE Link Level Simulator* [18]. The parameter setting is shown in Table 2.1. All presented simulation examples are made available for downloading.

2.6.1 Mean Square Error

Figure 2.4 shows the calculated MSE curves and the simulated estimation performance of the estimation scheme in Sect. 2.3. Generally speaking, the overall MSE is determined by the estimation in the frequency domain. The simulated curves follow the calculation except in the lower SNR region, due to the fact that the estimation errors from the time-domain estimation exceed the estimation range of the estimator

Table 2.1 Simulation parameters for results in Sect. 2.6

Parameter	Value
Channel bandwidth	1.4 MHz
FFT size (N_c)	128
No. data subcarriers	72
Subcarrier spacing	15 kHz
Carrier frequency	2.5 GHz
CP length (N_{cp})	[10, 9] (normal [11])
Transmission setting $N_R \times N_T$	1×1, 2×2
Transmission mode	Spatial multiplexing
Precoding	Identity
Channel model	ITU Pedestrian B [19]
CFO introduced (ε)	0, 0.14159 . . . subcarrier spacing
Channel knowledge	Perfect
Equalizer	Zero Forcing (ZF)

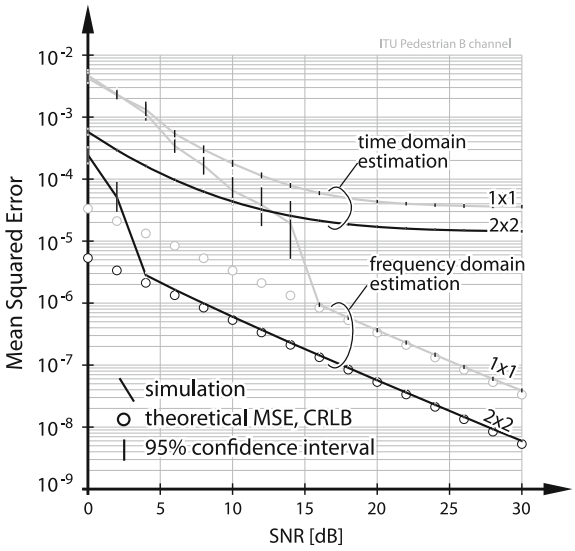

Fig. 2.4 Simulated and calculated MSE curves of the CFO estimation scheme

in the frequency domain. This effect, unfortunately, is not included in the theoretical analysis of the estimation performance.

2.6.2 Post-equalization Signal to Interference and Noise Ratio

In order to validate Eq. (2.27), we introduced 20 logarithmically spaced CFOs which are normalized to the subcarrier spacing, namely 15 kHz in LTE. Neither an estimation nor a compensation procedure was applied at this stage. For better visualization of the impact from the CFOs, the SNR is fixed at $\gamma = 30\,\text{dB}$. The resulting post-equalization SINR curves are plotted in Fig. 2.5 and compared to those obtained using Eq. (2.27).

Figure 2.5 shows that calculated results match well with those from the standard compliant simulation. This indicates that Eq. (2.27) can be used as a valid characterization of the system behavior.

2.6.3 Average Spectral Efficiency

The average spectral efficiency in Eq. (2.29) degrades as the post-equalization SINR decreases correspondingly. Given a series of deterministic CFOs, this degradation calculated using Eq. (2.29) is shown in Fig. 2.6. The results are based on 200 channel

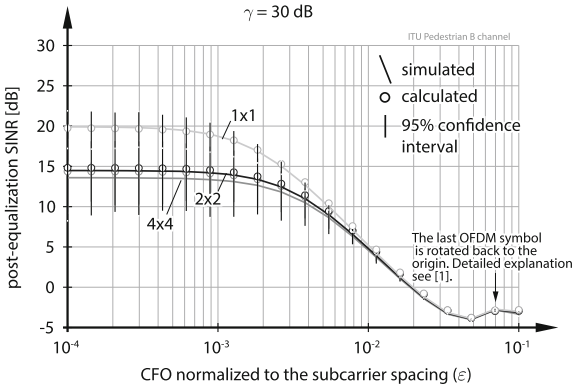

Fig. 2.5 Post-equalization SINR under increasing levels of residual CFOs in ITU Pedestrian B channel. The relatively large confidence intervals are due to the frequency selectivity over the data subcarriers

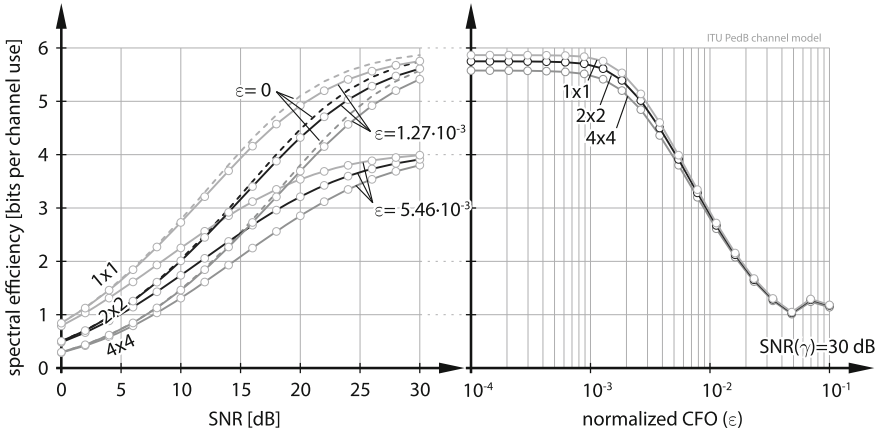

Fig. 2.6 Degradation in average spectral efficiency (per layer for the MIMO cases) due to the residual CFOs

realizations. For the MIMO cases, results are exhibited on a per transmission layer basis.

The subfigure on the left-hand side shows the theoretical degradation in average spectral efficiency subjected to a fixed CFO at different SNR levels. Two CFOs are introduced as examples where $\varepsilon = 1.27 \times 10^{-3}$ corresponds to 19.1 Hz and $\varepsilon = 5.46 \times 10^{-3}$ to 81.8 Hz given the subcarrier spacing 15 kHz. Compared to the zero-CFO case, it can be observed that the higher SNR region where higher efficiency is aimed, appears to be more sensitive to the CFO. Moreover, the impacts on Single-Input Single-Output (SISO) and MIMO systems are fairly equal on a per layer basis.

In the subfigure on the right-hand side, the SNR is fixed at $\gamma = 30$ dB in order to visualize the impact under CFOs of increasing magnitudes. The average spectral effi-

ciency starts to decrease around $\varepsilon = 1 \times 10^{-3}$, approximately. A similar behavior can be observed for the SISO and MIMO cases, although the average spectral efficiency per layer is slightly lower for the multiple antenna scenario due to the incremental noise enhancement from a ZF equalizer.

2.6.4 Coded Throughput Loss

As a comparison to the calculated BICM capacity, we simulated coded throughput of the LTE downlink. The fifteen MCSs indicated by Channel Quality Indicators (CQIs) are implemented, shown in Table 2.2. In the LTE downlink, User Equipments (UEs) provide wideband feedbacks to the eNodeB so that the MCS can be adapted to the actual channel quality. In our experiment, the CQI feedback is forced to be optimal by selecting the MCS that delivers the highest throughput for each channel realization.

Figures 2.7 and 2.8 exhibit the results obtained for a SISO and a 2×2 MIMO LTE DL. In the upper figures, coded throughputs of ideally synchronized transmissions are compared to the CFO-compensated case. With the CFO estimation scheme in [12] applied, the loss between the two cases is hardly visible, especially for the MIMO case. The corresponding achievable BICM capacity curves confirm such an

Table 2.2 Modulation scheme, Effective Code Rate (ECR) and efficiency for each of the Channel Quality Indicators (CQIs) of the LTE standard

CQI Index	Modulation	ECR	Data (bit/symbol)
0	Out of range		
1	4-QAM	0.08	0.15
2	4-QAM	0.12	0.23
3	4-QAM	0.19	0.38
4	4-QAM	0.30	0.60
5	4-QAM	0.44	0.88
6	4-QAM	0.59	1.18
7	16-QAM	0.37	1.48
8	16-QAM	0.48	1.91
9	16-QAM	0.60	2.41
10	64-QAM	0.46	2.73
11	64-QAM	0.55	3.32
12	64-QAM	0.65	3.90
13	64-QAM	0.75	4.52
14	64-QAM	0.85	5.12
15	64-QAM	0.93	5.55

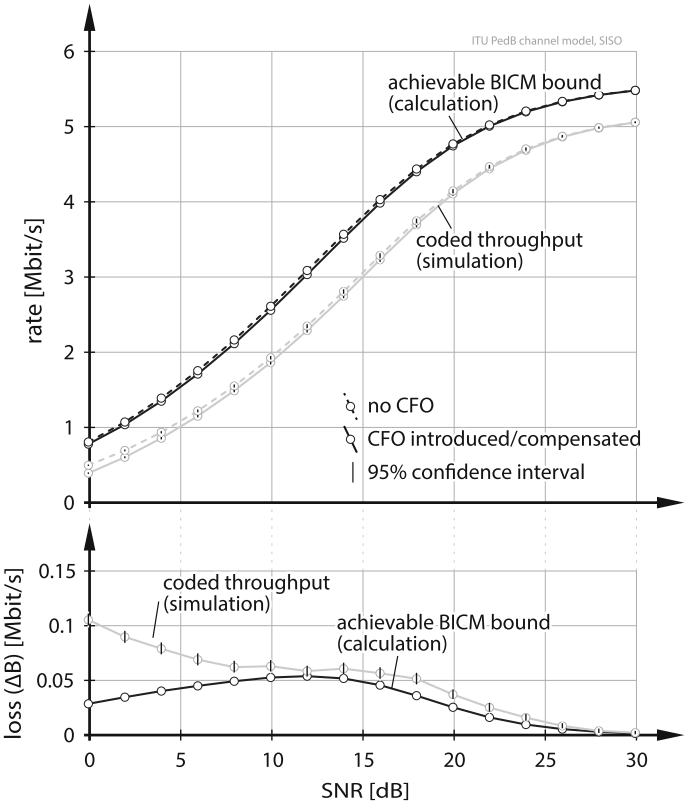

Fig. 2.7 Achievable BICM capacity and simulated coded throughput for an SISO LTE DL under CFO, 5000 subframes Monte Carlo simulation

observation. Note that there are absolute differences between calculated capacity curves and simulated coded throughput, it is due to the imperfect channel code.

In the lower subfigures of Figs. 2.7 and 2.8, the absolute coded throughput loss between the no-CFO and the CFO-compensated case are plotted. The absolute differences in the upper figure cancels out when calculating the relative loss. In the higher SNR region, it can be observed that the simulated coded throughput loss follows the trend of the analytical calculation. However, mismatches appear in the lower SNR region, which agrees with the MSE performance shown in Fig. 2.4. Since the theoretical MSE analysis fails to model the overflow in the frequency domain estimation, an increasing loss in the simulated overall throughput can be observed.

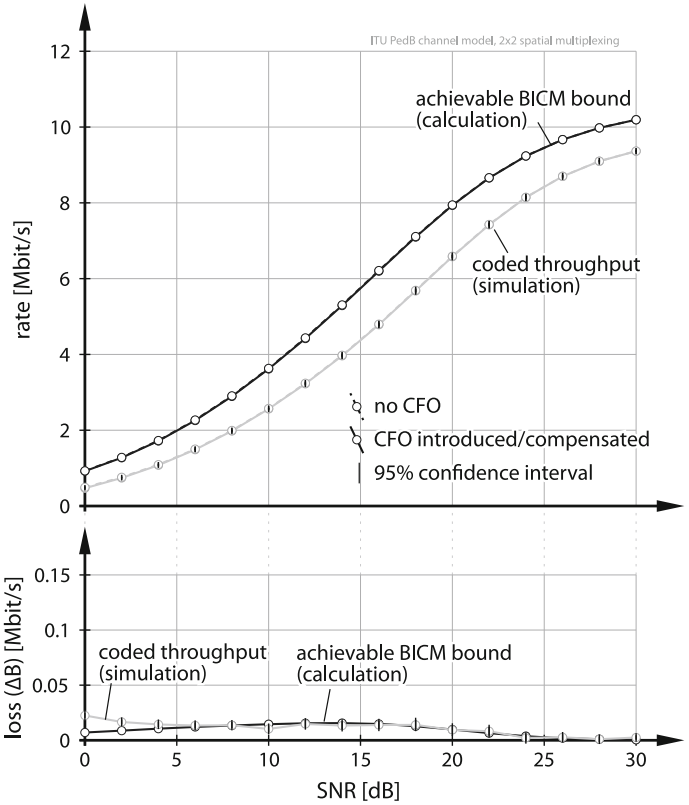

Fig. 2.8 Achievable BICM capacity and simulated coded throughput for a 2×2 spatial multiplexing LTE DL under CFO, 5000 subframes Monte Carlo simulation

2.7 Conclusion

In this chapter, we propose a throughput loss prediction model for a CFO-impaired LTE downlink. This model interconnects the three performance metrics, namely MSE, post-equalization SINR and the BICM capacity bound. Given the theoretical estimation performance of an arbitrary CFO estimator, the resulting performance loss in terms of coded throughput can be analytically determined with acceptable accuracy, avoiding extensive time-consuming link performance simulations. Validated by standard compliant link level simulations, a good agreement can be found. Since for a practical OFDM system, it is more important to find a sufficient estimator than the 'best', this model may serve as an evaluation tool for such purpose. Moreover, the example estimation scheme in [12] is shown to be sufficient for the LTE downlink with multiple antenna configuration in frequency selective scenarios.

References

1. B. Stantchev, G. Fettweis, Time-variant distortion in OFDM. IEEE Commun. Lett. **4**, 312–314 (2000)
2. J. Lee, H.-L. Lou, D. Toumpakaris, J. Cioffi, SNR analysis of ofdm systems in the presence of carrier frequency offset for fading channels. IEEE Trans. Wirel. Commun. **5**(12), 3360–3364 (2006)
3. K. Sathananthan, C. Tellambura, Probability of error calculation of OFDM systems with frequency offset. IEEE Trans. Commun. **49**(11), 1884–1888 (2001)
4. T. Pollet, M. Van Bladel, M. Moeneclaey, BER sensitivity of OFDM systems to carrier frequency offset and Wiener phase noise. IEEE Trans. Commun. **43**(234), 191–193 (1995)
5. P. Dharmawansa, N. Rajatheva, H. Minn, An exact error probability analysis of OFDM systems with frequency offset. IEEE Trans. Commun. **57**(1), 26–31 (2009)
6. L. Rugini, P. Banelli, BER of OFDM systems impaired by carrier frequency offset in multipath fading channels. IEEE Trans. Wirel. Commun. **4**(5), 2279–2288 (2005)
7. M. Krondorf, G. Fettweis, Bit error rate calculation for OFDM with synchronization errors in time and frequency selective fading channels, in *Proceedings of 13th European Wireless Conference (EW'07)*, Paris, France, Apr 2007
8. M. Krondorf, G. Fettweis, OFDM link performance analysis under various receiver impairments, in *EURASIP Journal on Wireless Communications and Networking*, vol. 2008, Article ID 145279, 2008
9. S. Schwarz, M. Šimko, M. Rupp, On performance bounds for MIMO OFDM based wireless communication systems, in *Proceedings of IEEE Signal Processing Advances in Wireless Communications SPAWC 2011*, June 2011
10. S. Caban, C. Mehlführer, M. Rupp, M. Wrulich, *Evaluation of HSDPA and LTE: From Testbed Measurements to System Level Performance*, 1st edn. (Wiley, New York, 2012)
11. Technical Specification Group Radio Access Network, E-UTRA; physical channels and modulation, 3GPP, Technical Report TS 36.211 Version 9.1.0, Mar 2010
12. Q. Wang, C. Mehlführer, M. Rupp, Carrier frequency synchronization in the downlink of 3GPP LTE, in *Proceeding of the 21st Annual IEEE International Symposium on Personal, Indoor and Mobile Radio Communications (PIMRC'10)* Istanbul, Turkey, 2010
13. M. Sandell, D. McNamara, S. Parker, Analysis of frequency-offset tracking in MIMO OFDM systems. IEEE Trans. Commun. **54**(8), 1481–1489 (2006). doi:10.1109/TCOMM.2006.878841
14. Q. Wang, M. Rupp, Analytical link performance evaluation of LTE downlink with carrier frequency offset, in *Conference Record of the 45th Asilomar Conference on Signals, Systems and Computers, 2011 (Asilomar-2011)*, Pacific Grove, USA, Nov. 2011
15. G. Caire, G. Taricco, E. Biglieri, Bit-interleaved coded modulation. IEEE Trans. Inf. Theory **44**(3), 927–946 (1998)
16. Technical Specification Group Radio Access Network, E-UTRA; physical layer procedures, 3GPP, Technical Report TS 36.211 Version 9.2.0, June 2010
17. G. Caire, G. Taricco, E. Biglieri, Capacity of bit-interleaved channels. Electron. Lett. **32**(12), 1060–1061 (1996)
18. C. Mehlführer, J.C. Ikuno, M. Šimko, S. Schwarz, M. Wrulich, M. Rupp, The Vienna LTE simulators—enabling reproducibility in wireless communications research. EURASIP J. Adv. Signal Process. (2011)
19. Members of ITU, Recommendation ITU-R M.1225: Guidelines for evaluation of radio transmission technologies for IMT-2000, International Telecommunication Union (ITU), Technical Report, 1997

http://www.springer.com/978-981-10-0616-6

The Vienna LTE-Advanced Simulators
Up and Downlink, Link and System Level Simulation
Rupp, M.; Schwarz, S.; Taranetz, M.
2016, XXXIV, 357 p. 139 illus., Hardcover
ISBN: 978-981-10-0616-6